$$-(1/24)(1+g_w)\bar{Z}e^{-4\bar{Z}}$$
$$-(1/32)[9+24g_w+16g_w^2]\bar{Z}^2e^{-\bar{Z}}$$
$$-(1/4)[3+7g_w+4g_w^2]\bar{Z}^2e^{-2\bar{Z}}$$
$$-(5/24)[1+2g_w+g_w^2]\bar{Z}^2e^{-3\bar{Z}} \quad (14e)$$

From Eqs. (3, 7, 13 and 14), the skin friction and heat transfer parameters f''_w and G'_w are given analytically by

$$f''_w = f_w + (1/2f_w)[1+\bar{\alpha}(1+2g_w)]$$
$$-(\bar{\alpha}^2/72f_w^5)[25+73g_w+54g_w^2]+\ldots \quad (15)$$

$$G'_w = f_w + (1/2f_w + 1/12f_w^3)[\bar{\alpha}(2+3g_w)-10]$$
$$-(\bar{\alpha}^2/2160f_w^7)[481+1340g_w+940g_w^2]+\ldots \quad (16)$$

Further, the velocity and enthalpy can also be calculated from the expressions

$$f' = f_w^2[\epsilon_1 F'_{11}+\epsilon_2 F'_{12}+\epsilon_1^2 F'_{21}+\epsilon_2^2 F'_{22}] \quad (17a)$$

$$G = [G_o+\epsilon_1 G_{11}+\epsilon_2 G_{12}+\epsilon_1^2 G_{21}+\epsilon_2^2 G_{22}] \quad (17b)$$

where

$$F'_{11} = 1-e^{-\bar{Z}}, \quad (18a)$$

$$F'_{12} = -(1/2)e^{-\bar{Z}}+(1/2)e^{-2\bar{Z}}+(1+g_w)\bar{Z}e^{-\bar{Z}}, \quad (18b)$$

$$F'_{21} = (1/2)[e^{-\bar{Z}}-e^{-2\bar{Z}}+\bar{Z}^2e^{-\bar{Z}}], \quad (18c)$$

$$F'_{22} = (1/144)[21+68g_w+36g_w^2]e^{-\bar{Z}}$$
$$+(1/24)[13+9g_w-6g_w^2]e^{-2\bar{Z}}$$
$$-(1/144)[95+122g_w]e^{-3\bar{Z}}$$
$$-(1/36)e^{-4\bar{Z}}+(1/24)[16+25g_w+6g_w^2]\bar{Z}e^{-\bar{Z}}$$
$$-(1/4)[6+12g_w+5g_w^2]\bar{Z}e^{-2\bar{Z}}$$
$$-(3/8)[1+g_w]\bar{Z}e^{-3\bar{Z}}$$
$$-(1/4)[3+7g_w+4g_w^2]\bar{Z}^2e^{-\bar{Z}}$$
$$-(1/2)[1+2g_w+g_w^2]\bar{Z}^2e^{-2\bar{Z}} \quad (18d)$$

Results and Conclusions

A comparison of the velocity and enthalpy profiles obtained from the above analytical solutions for $\bar{\alpha}=10.0$, $\bar{\beta}=0.0$, $g_w=0.0$, $f_w=2.5$, 5.0 with the numerical results obtained by quasilinearization[2] is made in Fig. 1. The critical wall parameters f''_w and G'_w calculated using Eqs. (15) and (16) are presented in Table 1, as compared with their values[2] obtained numerically. It is clear from the table as well as the figure that there is good agreement for large values of the suction parameter f_w. It might also be noted that, for $f_w=5.0$, the longitudinal velocity overshoot is very small.

Thus, the present investigation supplies analytical solution for the large suction case. Further, it reveals the fact that with very large rates of suction, the velocity overshoot can be almost eliminated even in flows with swirl characterized by velocity overshoot in the longitudinal direction.

References

[1] Back, L.H., "Flow and Heat Transfer in Laminar Boundary Layers with Swirl," *AIAA Journal*, Vol. 7, Sept. 1969, pp. 1781-89.

[2] Vimala, C.S., "Flow Problems in Laminar Compressible Boundary Layers," Ph.D. thesis, Jan. 1974, Ch. III, Dept. of Applied Mathematics, Indian Institute of Science, Bangalore, India.

[3] Nanbu, K., "Vortex Flow over a Flat Surface with Suction," *AIAA Journal*, Vol. 9, Aug. 1971, pp. 1642-43.

[4] Van Dyke, M., *Perturbation Methods in Fluid Mechanics*, Academic Press, New York and London, 1964.

Stability Predictions for Combustors with Acoustic Absorbers and Continuous Combustion Distributions

C. E. Mitchell* and M. R. Baer†
Colorado State University, Fort Collins, Colo.

Introduction

In an earlier paper[1] the authors presented an analytical technique suitable for determining the stability of combustors with partial length liners, and with an arbitrary number of planar sources of mass and energy distributed along the combustion chamber axis. This type of combustor model was chosen to approximate the actual continuous combustion distributions found in liquid rocket combustors. The approach led to a system of partial differential equations for the source free flow between the planar sources which could be solved under oscillatory conditions to determine the response of the planar sources necessary to sustain periodic oscillations. This type of analysis was chosen because a solution of the partial differential equations for the flowfield including mass, momentum, and energy sources was not available at that time.

This paper presents results of calculations performed in which the source terms are included in the analysis, and the realistic case of a continuous distribution of combustion sources in the axial direction is considered. These results exhibit a qualitative similarity to the multi-zone work. However, there is a substantial upward shift of the curves in all cases relative to the curves obtained in the earlier approximate analysis indicating a marked increase in predicted chamber stability. This difference in stability predictions between the two models is traced to some important damping effects associated with the distributed source terms which are neglected in the multi-zone model.

Analysis

If it is assumed (consistent with the earlier work[1]) that the combustion product gas is a single component calorically perfect inviscid and nonheat conducting gas, and that drag forces on the liquid propellant droplets and heat transfer between droplets and gas are negligible, then the conservation equations for the three-dimensional flowfield in the chamber may be written in the following nondimensional form:

$$\frac{\partial\rho}{\partial t}+\nabla\cdot\rho q = Q \quad \text{(continuity)}$$

$$\rho\frac{Dq}{Dt}-\frac{1}{\gamma}\nabla p = Q(q_f-q) \quad \text{(momentum)}$$

$$\frac{D\sigma}{Dt} = \frac{Q}{p}\left[h_{fs}-h-\frac{\gamma-1}{2}(2q\cdot q_f-q^2)\right] \quad \text{(entropy)} \quad (1)$$

The associated state equations are $p=\rho T$, $\rho=p^{1/\gamma}e^{-\sigma}$, and $T=h$. In these equations pressure, density, enthalpy, and temperature (p, ρ, h, T) are nondimensionalized through division by their steady-state values at the injector. Q represents the nondimensional volumetric mass source and is normalized by division by $(\bar{\rho}_o^*\bar{a}_o^*/R^*)$. The velocities q and q_f are made nondimensional through division by $\bar{a}_o^*$. The non-

Received December 2, 1974; revision received January 13, 1975. This research was sponsored by NASA Grant NGR06-002-095.

Index categories: Combustion Stability, Ignition, and Detonation; Wave Motion and Sloshing.

*Associate Professor, Department of Mechanical Engineering.

†Graduate Research Assistant, Department of Mechanical Engineering.

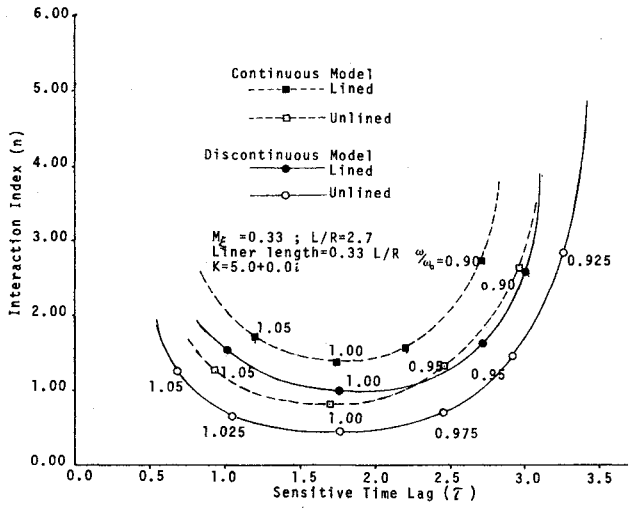

Fig. 1 Neutral stability curves comparing the continuous and discontinuous model predictions for a "ramp" type combustion distribution.

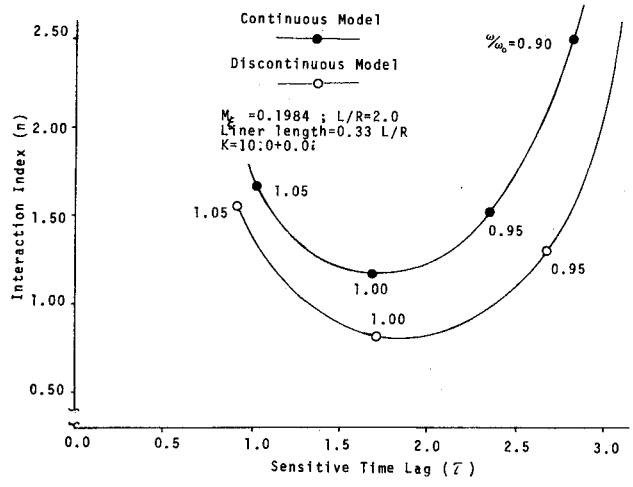

Fig. 2 Comparison of continuous and discontinuous model predictions for a vaporization rate controlled combustion distribution.

dimensionalizing factors for time and spatial coordinates are, respectively, $\bar{a}_o^*/R^*$ and $1/R^*$. The nondimensional entropy difference between the local value at a given time and the value at the injector in the steady state is designated by σ. It is the dimensional entropy difference divided by γC_v^*. Here asterisks indicate dimensional quantities, the subscript o designates a quantity evaluated at $z=0$, the subscript ℓ indicates a liquid droplet variable, and superposed bars are used to denote steady-state quantities.

In steady-state operation, one-dimensional flow in the z (axial) direction is assumed. Equations (1) then lead to the following results when the time derivatives are suppressed and the boundary conditions $\bar{u}=0$ at $z=0$ and $\bar{\rho}_\ell u_\ell = \bar{\rho}_E \bar{u}_E$ are applied (E represents nozzle entrance).

$$\bar{\rho}\bar{u} = \int_0^z \bar{Q}(z')dz'$$

$$\bar{p} = 1 + \gamma\bar{\rho}\bar{u}(\bar{u}_\ell - \bar{u})$$

$$\bar{p}/\bar{\rho} = \bar{h} = \bar{T} = 1 - (\gamma - 1/2)\bar{u}^2 \qquad (2)$$

Specification of the steady-state combustion source distribution, $\bar{Q}(z)$, in Eqs. (2) allows calculaton of $\bar{p}$, $\bar{\rho}$, $\bar{T}$, $\bar{u}$, and $\bar{\sigma}$ for arbitrary $\bar{Q}(z)$.

The time-dependent governing equations are linearized by assuming that the dependent variables can be represented as the sum of their steady-state values and small time dependent perturbation. Thus $p=\bar{p}+p'$, $\rho=\bar{\rho}+\rho'$, $q=\bar{u}+q'$, etc. Substitution of these representations into Eq. (1), and subtraction of the steady-state equations lead to the following linearized equations

$$\frac{1}{\gamma}\frac{\partial p'}{\partial t} + \bar{\rho}\nabla\cdot q' + \frac{1}{\gamma}p'\frac{d\bar{u}}{dz} + \frac{\bar{u}}{\gamma}\frac{\partial p'}{\partial z} + u'\frac{d\bar{\rho}}{dz} = Q' \qquad \text{(mass)}$$

$$\frac{\partial q'}{\partial t} + \nabla\bar{u}\,u' - \bar{u}\hat{e}_k x \nabla x q' + \nabla(p'/\gamma\bar{\rho}) = -\frac{\bar{Q}}{\bar{\rho}}q' + \frac{Q'}{\bar{\rho}}(\bar{u}_\ell - \bar{u})\hat{e}_k - \frac{\bar{Q}}{\bar{\rho}}\frac{p'}{\gamma\bar{\rho}}(u_\ell - \bar{u})\hat{e}_k \qquad \text{(momentum)} \quad (3)$$

Consistent with the multi-zone work σ' is taken to be zero in Eqs. (3). The boundary conditions are given by $\nabla q'\cdot n = \beta p'$ where β is the local admittance function. It is zero on the entire boundary surface of the combustor except at the nozzle entrance and over the portion of the cylindrical walls covered with acoustic absorbers.

If the velocity perturbation q' is represented as $\nabla\phi + \psi(\phi)$, then introduction of a Green's function allows the conversion of the governing equations and boundary conditions into two integral equations. The conversion follows in general the method used in Ref. (1) and will not be repeated here. The two equations are

$$\phi = \Omega_N + \int\int\int_V G_N F_1(\phi)dV + \int\int_S G_N F_2(\phi)ds$$

$$\omega - \eta_N^2 = \int\int\int_V \Omega_N F_1(\phi)dV + \int\int_S \Omega_N F_2(\phi)ds$$

where

$$-F_1(\phi) = A(z)\phi + B(z)\frac{\partial\phi}{\partial z} + C(z)\frac{\partial^2\phi}{\partial z^2} - \frac{1}{\bar{\rho}}\frac{\partial\bar{\rho}\psi_z}{\partial t} + Q'(\rho)^{1/2}$$

$$-F_2(\phi) = \gamma\beta\bar{\rho}\left\{i\omega\phi + \bar{u}\frac{\partial\phi}{\partial z} + \phi\frac{\bar{Q}}{\bar{\rho}}\right\}$$

Ω_N is the acoustic mode for the chamber which is assumed to be closest to the actual solution, and η_N is the associated eigenvalue for the mode, and $Q' = \bar{Q}\,n\,(1-e^{i\omega\tau})\,p'/\bar{p}$. n and τ are the interaction index and time lag of the sensitive time lag combustion response model used also in Ref. (1).

The integral equations are solved using a successive functional approximation technique. At each iteration step a functional form for ϕ is generated, and a corresponding value of n and τ is calculated. (ω is fixed in the calculation.)

Results and Conclusions

Results of calculations of the type previously described are compared with similar results obtained using the multi-zone approach in Figs. 1 and 2. Figure 1 compares the neutral stability curves for the approaches for a particular combustor configuration characterized by a steady-state combustion distribution in which the total mass generated increases linearly with axial length. This type of combustion distribution is called the "ramp" combustion distribution, following the terminology used in the earlier work. The length to radius ratio (L/R) for the combustor chosen is 2.7, and the nozzle entrance Mach number M_ξ is 0.33. Four neutral stability curves are shown, corresponding to lined and unlined chambers for the two different approaches. Areas inside

(above) any neutral stability core are predicted regions of linear instability, areas outside (below) the curve are regions of linear stability. The primary mode of oscillation is the first transverse mode characterized by a dimensionless acoustic frequency (ω_0) of 1.8413. The ratio ω/ω_0 is shown as a parameter along the stability limit curves. When the lined configuration is evaluated, the liner is taken to cover one third of the available wall area and to be located at the injector end. A specific acoustic impendance K, ($K=1/\gamma\beta$) of 5.0 is used to characterize the linear damping.

As can be seen in the figure, for either the lined or unlined case, the stability curve for the continuous model is displaced upward from the corresponding curve for the discontinuous (multi-zone) model. This implies that the discontinuous model predictions overestimates the regions of linear stability, and underestimates the linearly stable regions on the n,τ plane.

Apart from this relative displacement effect the curves for the two model are qualitatively quite similar. In both cases the addition of a liner causes a substantial stabilizing effect (upward shift of the neutral stability curve) relative to the unlined configuration. The minimum point on the curves in all cases occurs at a frequency close to ω_0. Finally it should be noted that the stabilizing displacement of the curve with liner addition is of the same order of magnitude as the stabilizing shift upward caused by using the improved model. This implies that a damping effect of the same order of magnitude as that produced by the liner is ignored in the multi-zone work.

Figure 2 is a similar type of plot for a different steady-state combustion distribution. The distribution in this case is one predicted using a vaporization controlled mass generation model. This distribution is described more fully in Ref. 1. Only lined configurations are considered in Fig. 2, with $L/R=2.0$, $K=10.0$, $M_\xi=0.1984$, and $\omega_0=1.8413$. The upward displacement of the stability limit curve for the continuous model relative to the discontinuous model, as well as a general qualitative similarity of the curves, is present also for this distribution.

With the results previously given in mind the question naturally arises as to what is neglected in the multi-zone model which accounts for its substantial underestimation of combustor stability. The answer can be found in a term which is present on the right-hand side of the momentum equation which exerts a considerable damping effect. Specifically, this term is $Q'(\bar{u}_\ell-\bar{u})/\bar{\rho}$, which is associated with the acceleration a propellant element experiences as it is generated. This is a source dependent term and does not appear in the differential equations for the multi-zone model. Neither is it accounted for in the matching (boundary) conditions between successive source free zones. As a result this important damping effect is lost in the multi-zone results and renders the predictions of that approach substantially and systematically in error.

Reference

[1] Baer, M. R., Mitchell, C. E., and Espander, W. R., "Stability of Partially Lined Combustors with Distributed Combustion," *AIAA Journal*, Vol. 12, April 1974, pp. 475-480.

Frequency Spectrum of Shells

A. V. Krishna A. Murty*
Indian Institute of Science, Bangalore, India

It is customary to neglect certain lower order terms in the formulation of thin-shell equations. The classical equation of motion for thin shells are given in textbooks.[1] The terms neglected normally, do not give rise to significant errors in the values of the natural frequencies when the thickness is small. However, when the thickness is large, the terms can change values of the natural frequencies significantly and also can modify the frequency spectrum. This Note is intended to show how the frequency spectrum gets modified when these lower order terms are included.

Received December 6, 1974.
Index categories: Structural Dynamic Analysis; LV/M Dynamics, Uncontrolled.

*Associate Professor, Department of Aeronautical Engineering.

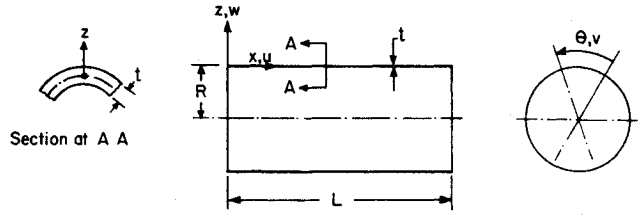

Fig. 1 Cylindrical shell.

Figure 1 shows a cylindrical shell of length L, radius R, and thickness t. Using the classical assumptions of normals to the middle surface before deformation remaining normal to the middle surface after deformation and assuming negligible shear strains, we have the strain displacements relationships in the form

$$\epsilon_{xx}=u_{,x}-z\,w_{,xx} \tag{1a}$$

$$\epsilon_{\theta\theta}=\frac{1}{R}v_{,\theta}+\frac{1}{R+z}w-\frac{z}{(R+z)R}w_{,\theta\theta} \tag{1b}$$

$$\epsilon_{x\theta}=\frac{R+z}{R}v_{,x}-\frac{2R+z}{R(R+z)}z\,w_{,x\theta}+\frac{u_{,\theta}}{R+z} \tag{1c}$$

The subscripts, θ, and, x indicate partial derivatives with respect to θ and x, respectively, and xx, etc., represent differentiation twice. The stress-strain relationships are

$$\sigma_{xx}=E'(\epsilon_{xx}+\nu\epsilon_{\theta\theta}) \tag{2a}$$

$$\sigma_{\theta\theta}=E'(\epsilon_{\theta\theta}+\nu\epsilon_{xx}) \tag{2b}$$

$$\sigma_{x\theta}=G\,\epsilon_{x\theta} \tag{2c}$$

with

$$E'=E/(1-\nu^2) \tag{3}$$

where E is the Young modulus, G is the shear modulus and ν is the Poisson ratio.

The displacement at any point in the shell $\bar{u}$, $\bar{v}$, $\bar{w}$ can be expressed in terms of the midplane displacements as

$$\bar{u}=u-z\,w_{,x}\qquad \bar{v}=v-z(w_{,\theta}-v)/R\qquad \bar{w}=w \tag{4}$$

Assuming sinusoidal oscillations, the maximum kinetic energy may be written as

$$T=\frac{\omega^2\rho}{2}\iiint(\bar{u}^2+\bar{v}^2+\bar{w}^2)\,(R+z)\,dx\,dz\,d\theta \tag{5}$$

and the maximum strain energy U_e as

$$U_e=\tfrac{1}{2}\iiint(\sigma_{xx}\epsilon_{xx}+\sigma_{\theta\theta}+\sigma_{x\theta}\epsilon_{x\theta})\,(R+z)\,dx\,dz\,d\theta \tag{6}$$

where ω is the natural frequency and ρ is the mass density of the shell. Using Eqs. (1-4) in Eqs. (5) and (6) and utilizing the principle of stationarity of the Lagrangian, the dynamical equations of motion may be obtained as

$$u_{,xx}+A_1u_{,\theta\theta}+A_2v_{,x\theta}+A_3w_{,x}+A_4u$$
$$+[A_5w_{,xxx}+A_6w_{,x\theta\theta}+A_7w_{,x}]=0 \tag{7a}$$